

# The quantum of action and finiteness of radiative corrections: Deconfining SU(2) Yang-Mills thermodynamics

Ralf Hofmann\* and Dariush Kaviani†

\* *Institut für Theoretische Physik  
Universität Heidelberg  
Philosophenweg 16  
69120 Heidelberg, Germany*

† *Institute for Particle Physics Phenomenology  
Durham University  
South Road  
Durham, DH1 3LE, United Kingdom*

## Abstract

The quantum of action  $\hbar$ , multiplying in certain powers perturbative vertices in 4D gauge theory, is related to the action of just-not-resolved selfdual and thermal gauge field configurations, calorons and anticalorons, of charge modulus unity. Appealing to the derivation of the effective theory for the deconfining phase of SU(2) Yang-Mills thermodynamics, we conclude that these vertex inducers convey a rapidly decreasing interaction strength between *fundamental* plane waves when the momentum transfer is increased away from the scale of maximal, *effective* resolution. This adds a deeper justification to the renormalization programme of perturbation theory which ignores the contribution to the partition function of nontrivially selfdual configurations. We also point out a connection between the QED fine-structure constant  $\alpha$  and the electric-magnetically dual of the effective gauge coupling in the deconfining phase, and we illustrate the workings of effective loops in the expansion of the pressure.

# 1 Introduction

Key experiments in all areas of subatomic and condensed matter physics, spanning over more than a hundred years and designed to investigate aspects of the microscopic interaction between electromagnetic radiation, charged particles, and collective excitations, prove that the quantum of action  $h = 6.63 \times 10^{-34}$  Js, introduced by Max Planck in understanding the spectral radiance of a black-body cavity through eventual appeal to the statistical thermodynamics of Ludwig Boltzmann [1], is a *universal* constant of Nature. Since its inauguration in 1900 the somewhat mysterious sneak-in of  $h$ , somehow being associated with ‘elementary regions’ or ‘free rooms for action’ [2], into the conception and development of quantum mechanics [1, 3, 4, 5, 6, 7] has been broaching a quest for deeper interpretation.

To understand the meaning of  $h$  as a mediator of indeterminism in fundamental interactions among propagating gauge fields, between gauge and charged matter fields, or in stationary binding physics could be of relevance in addressing as of yet poorly understood phenomena, for example those of 2D strongly correlated electron systems [8]. Quantum Mechanics and perturbatively accessed Quantum Field Theory are highly successful, accurate, and efficient. However, both suffer from problems of mere interpretation. While the measurement process in Quantum Mechanics, that is, the interaction of a macroscopic observer with the subatomic system under investigation, mysteriously and in a nonlocal, instantaneous way collapses the evolved wave function of the latter to an eigenstate of the operator-valued, measured quantity the need for renormalization in Quantum Field Theory, in addition to not easing the classical Euler-Lagrangian ambiguity inherent to the value of vacuum energy, is perceived by many as a necessary evil in putting perturbation theory to work. Fortunately, the predictive power of 4D gauge theories is not spoiled by the process of renormalization [9, 10], and radiatively introduced gauge anomalies can be canceled granting the consistency of the highly successful Standard Model of Particle Physics. Yet one may wonder whether the subtraction of infinities in the perturbative loop diagrams of gauge theories enjoys a deeper justification possibly supplied by full nonabelian gauge dynamics.

In the present paper we consider the (Euclidean) action of a fundamental, self-dual<sup>1</sup> gauge field configuration of topological charge modulus unity (trivial-holonomy Harrington-Shepard [11] or nontrivial-holonomy Lee-Lu-Kraan-Van-Baal caloron/anticaloron [12]) and scale parameter  $\rho$  in the deconfining phase of thermalized SU(2) Yang-Mills theory. The action of a caloron/anticaloron, that is *just not resolved* in the effective theory, is determined by the value of an effective coupling calculable in the according effective theory [13, 14, 15]. Recall that calorons and anticalorons are not resolved in this effective theory: Their contribution to effective dynamics fundamentally separates into a free part causing the emergence of an effective, inert, and spatially homogeneous adjoint scalar field  $\phi$  [13] and the effects of interactions with the propagating plane-wave sector (vanishing topological charge). It is a fact

---

<sup>1</sup>Here the term ‘selfdual’ stands for both negative and positive topological charge.

that the energy-momentum tensor vanishes on any selfdual gauge-field configuration, see for example [16], and hence also on calorons and anticalorons. Since the latter configurations thus do not propagate one may wonder [28] what their (potentially important) contribution to the thermodynamics of the high-temperature Yang-Mills gas actually is.

For the generic nonabelian gauge group  $SU(2)$  this question was addressed in [13, 14, 15], see also [16] for a summarizing presentation: While the emergence of  $\phi$  is sharply dominated by (large) calorons/anticolorons of radius  $\rho$  smaller than but comparable<sup>2</sup> to the scale of maximal resolution  $|\phi|$  in the effective theory [13] interactions between calorons/anticolorons and plane waves manifest in a two-fold way effectively. First, there are small holonomy changes, induced through momentum transfers by plane-wave fluctuations that are largely off their free mass shell<sup>3</sup>, which generate negative ground-state pressure by virtue of a pure-gauge configuration of the effective gauge field [14, 16, 17]. Second, as we shall make explicit in this paper, just-not-resolved calorons/anticolorons are responsible for pointlike vertices, associated with their dissociation into screened but unresolved monopole-antimonopole pairs on one hand [18] and a rapidly converging loop expansion in the effective theory [19, 20, 21, 22]. We will make clear that this loop expansion, which can naively be organized into an expansion in powers of  $\hbar \equiv \frac{h}{2\pi}$ , turns out to be a more subtle expansion. Still, the action of a just-not-resolved caloron or anticaloron, which introduces a vertex for effective plane waves, turns out to be  $\hbar$ .

Calculating loops in effective variables yields a quantitative description of collective effects as induced by fundamental field configurations [18, 23, 24, 25]. Moreover, since the fields of the effective theory and their interactions do only depend on the contributions of large calorons/anticolorons we would conclude that, on a fundamental level, the mediation of interactions between unresolved off-shell plane-wave fluctuations by calorons/anticolorons (vertices) dies off rapidly with decreasing  $\rho$ . As a consequence, there are *no* interactions with potentially large momentum transfers deep within the unresolved physics. We tend to interpret this as a justification for the perturbative renormalization procedure in nonabelian gauge theories. Finally, it is instructive to illustrate the technicalities of the effective loop expansion to contrast it with renormalized perturbation theory.

The paper is organized as follows. Because our subsequent discussion relies on it we review in Sec. 2.1 the emergence of an inert, adjoint scalar field  $\phi$  by a spatial coarse-graining over noninteracting calorons and anticalorons of charge modulus unity within the deconfining phase of  $SU(2)$  Yang-Mills thermodynamics. For the same reason, we re-derive in Sec. 2.2 the thermodynamically consistent solution for the temperature dependence of the effective gauge coupling  $e$ . In Sec. 2.3 we identify the Euclidean action of just-not-resolved calorons and anticalorons with the quan-

---

<sup>2</sup>The integral over  $\rho$  in the space-averaged two-point function of the fundamental field strength defining in singular gauge the kernel  $\mathcal{K}$  of a differential operator  $D$ , with  $\phi \in \mathcal{K}$ , exhibits a cubic dependence on the cutoff when the latter is comparable to  $|\phi|^{-1}$ , see [13] and Sec. 2.1 below.

<sup>3</sup>All unresolved plane-wave fluctuations are at least by  $|\phi|$  off their free mass shell.

tum of action  $\hbar$  and deduce, by virtue of the dimensionlessness of the fine-structure constant  $\alpha$ , an interpretation of the fundamental unit of electric charge in terms of the dual to the effective  $SU(2)$  gauge coupling in the deconfining phase. Sec. 2.4 discusses the implications of the action of a just-not-resolved caloron or anticaloron being associated with a local vertex. Namely, from the derivation of the effective theory we learn that such vertices are sharply suppressed with increasing momentum transfer (or decreasing caloron/anticaloron radius  $\rho$ ) yielding, at *any* externally prescribed resolution, finite answers for all radiative processes. Focusing on the example of QED, Sec. 2.5 discusses how just-not-resolved calorons and anticalorons of  $SU(2)_{\text{CMB}}$  may induce local vertices between the plane waves belonging to electrically charged particles and propagating electromagnetic waves. To point out the contrast to renormalized perturbation theory, where the emergence of a scalar field associated with the maximal resolution and induced by the topologically nontrivial sector can not occur due to an a priori restriction to the plane-wave sector, Sec. 3 discusses the technicalities of the effective loop expansion of the pressure. Namely, we review the Feynman rules and constraints on loop variables and apply them to the (numerical) computation of three- and two-loop contributions to the pressure.

## 2 Selfduality, propagating fields, and powers of $\hbar$

### 2.1 Inert adjoint scalar field $\phi$ and effective action

In [13] the following definition for the kernel  $\mathcal{K}$  of the differential operator  $D$  associated with  $\phi$ 's equation of motion in the deconfining phase of  $SU(2)$  Yang-Mills thermodynamics was shown to be unique:

$$\mathcal{K} \equiv \{\hat{\phi}^a\} \equiv \sum_{C,A} \text{tr} \int d^3x \int d\rho t^a F_{\mu\nu}(\tau, \mathbf{0}) \{(\tau, \mathbf{0}), (\tau, \mathbf{x})\} F_{\mu\nu}(\tau, \mathbf{x}) \{(\tau, \mathbf{x}), (\tau, \mathbf{0})\} , \quad (1)$$

where

$$\begin{aligned} \{(\tau, \mathbf{0}), (\tau, \mathbf{x})\} &\equiv \mathcal{P} \exp \left[ i \int_{(\tau, \mathbf{0})}^{(\tau, \mathbf{x})} dz_\mu A_\mu(z) \right] , \\ \{(\tau, \mathbf{x}), (\tau, \mathbf{0})\} &\equiv \{(\tau, \mathbf{0}), (\tau, \mathbf{x})\}^\dagger , \end{aligned} \quad (2)$$

and  $F_{\mu\nu}$  denotes the fundamental field-strength tensor. The Wilson lines in Eq. (2) are calculated along the straight spatial line connecting the points  $(\tau, \mathbf{0})$  and  $(\tau, \mathbf{x})$ , and  $\mathcal{P}$  demands path-ordering symbol. (The euclidean time coordinate is  $\tau$ .) In (1) the sum is over a noninteracting caloron ( $C$ ) and a noninteracting anticaloron ( $A$ ) of trivial holonomy and topological charge modulus unity, and  $\rho$  denotes their (instanton) scale parameter. Both caloron and anticaloron are spatially centered at  $\mathbf{z}_{C,A} = 0$ , for a discussion of the distribution of action density in dependence of  $\rho/\beta$  ( $\beta \equiv 1/T$ ,  $T$  temperature) see [27]. In evaluating the integrals on the right-hand

side of Eq. (1), one notices that only the magnetic-magnetic correlation gives rise to a nonvanishing result. Going over to spherical coordinates, both the unconstrained integration over  $r \equiv |\mathbf{x}|$  and  $\rho$  generate diverging multiplicative constants in front of a rapidly saturating sinusoidal time dependence separately arising from both the caloron as well as the anticaloron contribution. On the other hand, the azimuthal angular integration yields a multiplicative zero [13, 16]. Together this generates an undetermined real prefactor which is one of the parameters spanning the kernel  $\mathcal{K}$  of a uniquely determined second-order linear operator  $D$ . More specifically, one arrives at the following expression for the kernel  $\mathcal{K} = \{\hat{\phi}^a\}$  of differential operator  $D$

$$\{\hat{\phi}^a\} = \{\Xi_C(\delta^{a1} \cos \alpha_C + \delta^{a2} \sin \alpha_C) \mathcal{A}(2\pi(\hat{\tau} + \hat{\tau}_C)) + \Xi_A(\delta^{a1} \cos \alpha_A + \delta^{a2} \sin \alpha_A) \mathcal{A}(2\pi(\hat{\tau} + \hat{\tau}_A))\} \quad (a = 1, 2, 3), \quad (3)$$

where  $\Xi_C$ ,  $\Xi_A$ ,  $\hat{\tau}_C$ , and  $\hat{\tau}_A$  are undetermined real parameters, and  $\alpha_C$ ,  $\alpha_A$  are angles that reflect the freedom of a global gauge choice. The amplitude function  $\mathcal{A}$  is given as

$$\mathcal{A}(2\pi\hat{\tau}) = \frac{32\pi^7}{3} \int_0^\xi d\hat{\rho} \hat{\rho}^4 \left[ \lim_{\hat{r} \rightarrow \infty} \sin(2\hat{g}(\hat{\tau}, \hat{r}, \hat{\rho})) \right] \frac{\pi^2 \hat{\rho}^2 + \cos(2\pi\hat{\tau}) + 2}{(2\pi^2 \hat{\rho}^2 - \cos(2\pi\hat{\tau}) + 1)^2}, \quad (4)$$

where  $\xi$  represents a cutoff for the  $\rho$  integration in units of  $\beta$ . (All quantities of dimension length are made dimensionless by division with  $\beta$  and are denoted by a hat symbol). Function  $\hat{g}$  saturates rapidly to a finite limit as  $\hat{\rho}, \hat{r} \rightarrow \infty$ , the integral over  $\hat{\rho}$  in Eq. (4) diverges cubically for  $\xi \rightarrow \infty$ , and function  $\mathcal{A}(2\pi\hat{\tau})$  rapidly approaches  $\text{const}_\infty \times \xi^3 \sin(2\pi\hat{\tau})$ . Numerically, one obtains  $\text{const}_\infty = 272.018$ . To summarize, the kernel  $\mathcal{K}$ , which uniquely determines operator  $D$  as  $D \equiv \partial_\tau^2 + \left(\frac{2\pi}{\beta}\right)^2$ , is sharply dominated by contributions of the  $\hat{\rho}$  integration that lie in the vicinity of the upper limit  $\xi$ .

Operator  $D$  is explicitly dependent on temperature and thus, by itself, cannot be taken to be associated with a temperature-independent effective action<sup>4</sup> for the field  $\phi$ . The latter, however, arises by allowing a potential  $V$  to absorb the explicit temperature dependence introduced by  $D$ . Appealing to the BPS condition inherited from the selfduality of the fundamental gauge-field configurations entering into the definition (1), a first-order equation for  $\phi$  is derived whose solution is parametrized by one constant of integration – the Yang-Mills scale  $\Lambda$ . Perturbative renormalizability [9, 10], constraining the interactions between effective plane-wave fields  $a_\mu = a_\mu^a t_a$  ( $t^a$  with  $a = 1, 2, 3$  the generators of  $\text{SU}(2)$  in fundamental representation, normalized to  $\text{tr } t^a t^b = \frac{1}{2} \delta^{ab}$ ), gauge invariance, and the fact that the field  $\phi$  cannot, by definition, absorb or emit any energy-momentum yield the following unique result for the effective Euclidean action density  $\mathcal{L}_{\text{eff}}$  [13, 16]

$$\mathcal{L}_{\text{eff}}[a_\mu] = \text{tr} \left( \frac{1}{2} G_{\mu\nu} G_{\mu\nu} + (D_\mu \phi)^2 + \frac{\Lambda^6}{\phi^2} \right), \quad (5)$$

---

<sup>4</sup>This action is not explicitly temperature dependent because the weights of selfdual configurations in the fundamental partition function are solely associated with their topological charges.

where  $G_{\mu\nu} = \partial_\mu a_\nu - \partial_\nu a_\mu - ie[a_\mu, a_\nu] \equiv G_{\mu\nu}^a t_a$  denotes the field strength for gauge field  $a_\mu$ ,  $D_\mu \phi = \partial_\mu \phi - ie[a_\mu, \phi]$ , and  $e$  is the effective gauge coupling to be determined, see Sec. 2.2. Action density  $\mathcal{L}_{\text{eff}}$  yields a highly accurate tree-level ground-state estimate and, as easily deduced in unitary gauge  $\phi = 2|\phi|t_3$ , tree-level mass  $m = 2e|\phi| = 2\sqrt{\frac{\Lambda^3}{2\pi T}}$  for propagating gauge modes  $a_\mu^{1,2}$  rendering them thermal quasiparticles.

## 2.2 Thermodynamical consistency

For action density  $\mathcal{L}_{\text{eff}}$  to be thermodynamically consistent implied quantities like pressure and energy density must be related by Legendre transformations. On the level of free thermal fluctuations<sup>5</sup> we obtain the following evolution equation [14]

$$\partial_a \lambda = -\frac{24\lambda^4 a}{(2\pi)^6} \frac{D(2a)}{1 + \frac{24\lambda^3 a^2}{(2\pi)^6} D(2a)}. \quad (6)$$

Eq. (6) is equivalent to [26]

$$1 = -\frac{24\lambda^3}{(2\pi)^6} \left( \lambda \frac{da}{d\lambda} + a \right) a D(2a), \quad (7)$$

where  $\lambda \equiv \frac{2\pi T}{\Lambda}$ ,  $a \equiv \frac{m}{2T}$  and thus  $a = 2\pi e\lambda^{-3/2}$ , and  $D(y) \equiv \int_0^\infty dx \frac{x^2}{\sqrt{x^2+y^2}} \frac{1}{e^{\sqrt{x^2+y^2}} - 1}$ . The right-hand side of Eq. (6) is negative definite. As a consequence, its solution  $\lambda(a)$  is strictly monotonic decreasing and so is its inverse  $a(\lambda)$ . Hence there is a regime in temperature  $\lambda > \lambda_1$  where  $a(\lambda) < 1$ , and Eq. (7) can be approximated as

$$1 = -\frac{\lambda^3}{(2\pi)^4} \left( \lambda \frac{da}{d\lambda} + a \right) a. \quad (8)$$

The solution to Eq. (8), subject to the initial condition  $a(\lambda_i) = a_i \ll 1$ , is given as

$$a(\lambda) = 4\sqrt{2}\pi^2 \lambda^{-3/2} \left( 1 - \frac{\lambda}{\lambda_i} \left[ 1 - \frac{a_i^2 \lambda_i^3}{32\pi^4} \right] \right)^{1/2}. \quad (9)$$

Thus for  $\lambda_1 < \lambda \ll \lambda_i$  function  $a(\lambda)$  runs into the attractor  $a(\lambda) = 4\sqrt{2}\pi^2 \lambda^{-3/2}$ . Using  $a \equiv \frac{m}{2T} = 2\pi e\lambda^{-3/2}$ , this attractor corresponds to the plateau  $e \equiv \sqrt{8}\pi$ . Because the attractor increases with decreasing  $\lambda$  the condition  $a \ll 1$  will be violated at small temperatures. The estimate  $14.61 > \lambda_1$  is obtained by setting the attractor equal to unity. Lowering  $\lambda$  further, the solution to the full Eq. (7) runs into a thin pole at  $\lambda_c$  of the form [16]

$$e(\lambda) = -4.59 \log(\lambda - \lambda_c) + 18.42, \quad (10)$$

---

<sup>5</sup>In the physical unitary-Coulomb gauge  $\phi = 2|\phi|t_3$ ,  $\partial_i a_i^3 = 0$  the off-shellness of quantum fluctuations in the field  $a_\mu$  is constrained by the maximal resolution  $|\phi|$ . Their contribution turns out to be negligible compared to that of thermal fluctuations [14, 16].

where  $\lambda_c = 13.87$ . Now, setting the upper integration limit  $\xi$  in Eq. (4) equal to  $1/(\beta|\phi|^{-1})$  and invoking  $\lambda_c = 13.87$ , yields  $\xi \geq (13.87)^{3/2}/(2\pi) \sim 8.22$ . But the approach of function  $\mathcal{A}(2\pi\hat{\tau})$  to a sine is perfect for  $\xi \sim 8.22$  [13, 16], and for  $\xi \sim 8.22$  the integral in Eq. (4) is strongly dominated by its upper limit. We conclude that calorons and anticalorons that are just not resolved dominate the emergence of the field  $\phi$  and its consequences for the effective gauge dynamics (adjoint Higgs mechanism and thermal ground state estimate).

The divergence of  $e$  at  $\lambda_c$  initiates a transition to a phase where thermal quasi-particles decouple, the ground state is a condensate of magnetic monopoles, and a formerly massless gauge mode acquires mass by the dual Meissner effect [14, 16].

We conclude that *almost everywhere* in the deconfining phase the effective coupling assumes the constant value  $e \equiv \sqrt{8\pi}$ .

## 2.3 Counting of powers of $\hbar$ and action of just-not-resolved caloron

Concerning the counting of powers in  $\hbar$ , loop expansions in the effective theory are carried out as in conventional perturbation theory. Additional subtleties arise because of the existence of a maximal resolution  $|\phi|$  which enforces constraints on momentum transfers in four-vertices and on the off-shellness of the massless mode. These constraints have an obvious form in physical unitary-Coulomb gauge, see Sec. 3. To make the power counting in  $\hbar$  most explicit, we work in units where  $k_B = c = \epsilon_0 = \mu_0 = 1$  but  $\hbar$  is re-instated as an action. (So far we have worked in supernatural units  $\hbar = c = k_B = 1$ ). The (dimensionless) exponential

$$- \frac{\int_0^\beta d\tau d^3x \mathcal{L}'_{\text{eff}}[a_\mu]}{\hbar}, \quad (11)$$

in the weight belonging to fluctuating fields in the partition function<sup>6</sup> thus can, in unitary gauge, be re-cast as

$$- \int_0^\beta d\tau d^3x \text{tr} \left( \frac{1}{2} (\partial_\mu \tilde{a}_\nu - \partial_\nu \tilde{a}_\mu - ie\sqrt{\hbar} [\tilde{a}_\mu, \tilde{a}_\nu])^2 - e^2 \hbar [\tilde{a}_\mu, \tilde{\phi}]^2 \right), \quad (12)$$

where  $\tilde{a}_\mu \equiv a_\mu/\sqrt{\hbar}$  and  $\tilde{\phi} \equiv \phi/\sqrt{\hbar}$  are assumed to not depend on  $\hbar$  [29], see also [30]. Notice that because of the terms  $\propto \hbar^0$  in (12) the unit of  $\tilde{a}_\mu$  is  $\text{length}^{-1}$ . Thus the coupling  $e$  must have the unit of  $1/\sqrt{\hbar}$  (and the unit of  $\tilde{\phi}$  is also  $\text{length}^{-1}$ ). Together with the results reviewed in Sec. 2.2 we thus have

$$e = \frac{\sqrt{8\pi}}{\sqrt{\hbar}} \quad (13)$$

---

<sup>6</sup>Recall that  $\phi$  is inert. As a consequence, the factor, whose exponent is the potential-part of the effective action, can be pulled out of the partition function and needs not be considered in a discussion of the effective loop expansion.

almost everywhere in the deconfining phase. Because fundamental field configurations are smoothly connected to the effective dynamics<sup>7</sup> the action  $S_{C,A;\rho\sim|\phi|^{-1}}$  of a just-not-resolved caloron/anticaloron reads

$$S_{C,A;\rho\sim|\phi|^{-1}} = \frac{8\pi^2}{e^2} = \hbar. \quad (14)$$

Equation (14) has implications. First, it suggests that the quantum of action  $\hbar$ , whose introduction in (11) is motivated by the laws of Quantum Mechanics and which should enable a systematic accounting of quantum corrections (number of loops) in the effective theory, coincides with the Euclidean action of a just-not-resolved selfdual (classical) field configuration whose topological charge is fixed to be of modulus unity [13, 16]. That is, the reason why  $\hbar$  really is a constant can be traced to the universal constancy of  $e$  (almost no dependence on  $T$  and no dependence on the specific Yang-Mills scale  $\Lambda$  of a given SU(2) gauge theory) and the fact that only charge-modulus-unity calorons/anticalorons contribute to the effective thermodynamical consistency of interacting, fundamental topological and plane-wave configurations [13]. Moreover, rather than multiplying first and second powers of  $\hbar^{1/2}$  onto the powers  $e$  and  $e^2$  of an a priori unknown coupling constant  $e$  in three- and four-vertices of a Yang-Mills theory we would infer that these vertices exist only because of the presence of just-not-resolved calorons and anticalorons. Second, for the fine-structure constant  $\alpha$  of Quantum Electrodynamics (QED) to be dimensionless,

$$\alpha = N^{-1} \frac{g^2}{4\pi\hbar}, \quad (15)$$

the coupling  $g$  in Eq. (15) must have the unit of  $\sqrt{\hbar}$ . ( $N^{-1}$  denotes a numerical factor related to the mixing of the massless modes belonging to several SU(2) groups, see [16, 31].) This is guaranteed if  $g$  is taken to be the electric-magnetically dual coupling to  $e$ :

$$g = \frac{4\pi}{e} \propto \sqrt{\hbar}. \quad (16)$$

That is, a magnetic monopole liberated by the dissociation of a large-holonomy SU(2) caloron and other incarnations of this magnetic charge in the preconfining and confining phase<sup>8</sup> are interpreted as *electric* charges in the real world. Third, by virtue of Eq. (13) the factors  $e\sqrt{\hbar}$  and  $e^2\hbar$  in (12) do not depend on  $\hbar$ . Thus, by assumption the weight of the partition function associated with the effective theory is independent of  $\hbar$ , and thus the effective loop expansion is *not* an expansion in powers of  $\hbar$ . This is in contrast to renormalized perturbation theory where the value of the coupling is a priori unknown: The perturbative coupling constant needs to be determined by an empirical boundary condition.

---

<sup>7</sup>The spatial coarse-graining rapidly saturates:  $\frac{|\phi|^{-1}}{\beta} \geq 8.221 \times \left(\frac{\lambda}{\lambda_c}\right)^{3/2}$  and practically no alteration of  $\phi$ 's time dependence occurs when varying  $r, \rho \sim |\phi|^{-1}$  [16].

<sup>8</sup>For example, the isolated charge situated in the center of the flux eddy associated with the selfintersection of a center-vortex loop in the confining phase [16, 32], see also discussion in Sec. 2.5.



## 2.4 Unresolved, interacting plane waves: Local vertices by caloron/anticaloron mediation

From the results of Sec. 2.3 and the facts reviewed in Sec. 1 we may conclude that in the effective theory the pure-gauge configuration, associated with the a priori estimate of the thermal ground state, describes the collective effect of interacting (typically small-holonomy) calorons/anticalorons of action  $\hbar$  that are just not resolved. Recall that the holonomy of calorons/anticalorons is elevated from small to large by effective plane-wave interactions which collectively account for dissociation into screened but unresolved magnetic monopole-antimonopole pairs [18, 33]. Extrapolating the finding, that it is unresolved calorons/anticalorons which induce local vertices between plane waves, deeply into the unresolved domain, we would by the (ultraviolet as well as infrared) finiteness of all quantities calculable in the effective theory and the fact that the emergence of the field  $\phi$  is dominated by just-not-resolved calorons/anticalorons reason (cubic dependence of the prefactor of  $\phi$ 's time dependence on the cutoff for the  $\rho$  integration, see Eq. (4) and [13, 16]) that the strength of interactions between fundamental plane waves, which are largely off their free mass shell, rapidly ceases with increasing momentum transfer. Recall that the effective pure-gauge configuration of the thermal ground-state estimate, which collectively describes these interactions, is *sourced* by the field  $\phi$  [14, 15, 16]. But again, the content of fundamental charge-modulus unity selfdual gauge-field configuration in  $\phi$  is *strongly dominated* by those calorons/anticalorons that are *just not resolved*.

The point of view, see Fig. 1, that the emergence of local vertices between plane waves in a Quantum Yang-Mills theory is a consequence of the existence of nonpropagating, topologically stabilized and selfdual Euclidean field configurations of the same theory, compares in an interesting way to pure perturbation theory where such local vertices are taken for granted<sup>9</sup>. Namely, while perturbation theory requires a renormalization programme to sweep ultraviolet divergences under the carpet the latter do not occur to begin with when vertices are understood to be induced by unresolved, nonpropagating, topological, and selfdual field configurations: Because potential plane-wave fluctuations, that are extremely off-shell compared to an externally imposed resolution<sup>10</sup>, do not interact they are not generated in the first place. To the authors' minds this situation does by no means contradict the renormalization programme of perturbation theory but rather supplies it with a deeper justification: The subtraction of infinities in perturbative loop diagrams, which ignore the presence of the nontrivially selfdual sector of gauge-field configurations, simulates the nonoccurrence of such divergences in the full Yang-Mills theory.

---

<sup>9</sup>For the effective and local interaction between fundamentally charged chiral fermions via their zero modes, which are localized on instantons, the 't Hooft vertex represents an example of plane waves interacting by the mediation of selfdual gauge-field configurations [34, 35].

<sup>10</sup>In the case of thermodynamics this resolution is prescribed by temperature to be  $|\phi|$ .

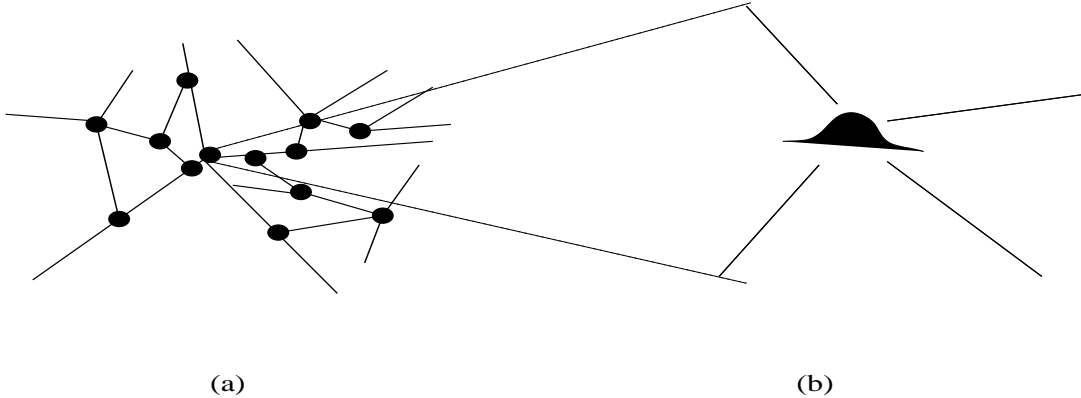


Figure 1: (a) Plane waves (lines) of a Yang-Mills theory interacting via local vertices (solid circles), (b) generation of a vertex (local crumble within the ensemble of non-interacting plane waves) by a nonpropagating and selfdual gauge-field configuration of topological charge modulus unity in the same Yang-Mills theory.

## 2.5 Gauge-field-matter interactions

So far we have discussed the situation of a pure  $SU(2)$  Yang-Mills theory. The undisputed successes of perturbatively accessed QED in particular (and the Standard Model of Particle Physics as a whole) demand to put the results of Secs. 2.3 and 2.4 into the perspective of electrically charged particle interacting with photons. Let us undertake a perhaps speculative discussion of the situation in QED.

To attribute caloron/anticaloron mediation to a QED vertex, the  $U(1)$  gauge group must be considered a dynamically broken  $SU(2)$ . As explained in Sec. 1 and investigated in [13, 14, 15, 16] this gauge-symmetry breaking is collectively mediated by calorons and anticalorons in terms of the field  $\phi$ . In [36] the critical temperature  $T_c$  of this  $SU(2)$  theory (and thus its Yang-Mills scale) was, by interpretation of the observed low-frequency excess in line temperature (see references in [36]), extracted to be the present baseline temperature 2.725 Kelvin of the Cosmic Microwave Background (CMB). Thus the name  $SU(2)_{\text{CMB}}$ .

Radiative corrections in QED are organized into a power series in the fine-structure constant  $\alpha$ . As already mentioned in Sec. 2.3  $\alpha$  measures the strength of interaction of the massless mode of  $SU(2)_{\text{CMB}}$  (the propagating photon) with a screened yet unresolved monopole [18]. Such a monopole becomes isolated and thus resolvable when trapped in the core of the selfintersection of a center-vortex loop [37]. Notice that in the presence of propagating photons a center-vortex loop of selfintersection number unity is the only absolutely stable degree of freedom in the confining phase of an  $SU(2)$  Yang-Mills theory. (The nonselfintersecting species shrinks to a round point [32] and vortex loops of intersection number larger than unity decay by charge annihilation or repulsion [37, 38].) For the  $SU(2)_{\text{CMB}}$  photon to see the charge of a monopole belonging to another  $SU(2)$  theory, which presently

is in its confining phase, the two theories must mix. So the crumble in the photonic plane wave, induced by the presence of the electric charge of, say, an electron, occurs by having the latter couple to its very massive photon (confining phase) which in turn mixes into the  $SU(2)_{\text{CMB}}$  plane wave by caloron/anticaloron mediation of the latter theory. Recall that, according to the results of Sec. 2.3, this mediation is accompanied by a unit  $\hbar$  of ‘free rooms for action’.

Interestingly, since the QED action, involving the electron field  $\psi$  and  $a_\mu^3$ , is given as [29]

$$S_{\text{QED}} = \int d^4x \left( \bar{\psi} (\gamma^\mu (i\hbar \partial_\mu - g a_\mu^3) - m) \psi \right), \quad (17)$$

where now  $\psi$ ,  $\tilde{m} \equiv \frac{m}{\hbar}$ , and  $\tilde{a}_\mu^3$  are considered independent of  $\hbar$ , one arrives at

$$- \frac{S_{\text{QED}}}{\hbar} = - \int d^4x \left( \bar{\psi} (\gamma^\mu (i\partial_\mu - \frac{1}{\sqrt{\hbar}} g a_\mu^3) - \tilde{m}) \psi \right). \quad (18)$$

By virtue of Eq. (16) we would thus conclude from Eq. (18) that the interaction  $\frac{1}{\sqrt{\hbar}} g \bar{\psi} \gamma^\mu a_\mu^3 \psi$  does not exhibit an  $\hbar$  dependence. So even in QED the loop expansion can no longer be considered an expansion in powers of  $\hbar$  if the vertex is interpreted to be induced by a caloron/anticaloron of  $SU(2)_{\text{CMB}}$ .

### 3 Effective and irreducible, planar 3-loop corrections

After ‘scratching into unresolved physics’ in Sec. 2 to associate interactions between plane waves with the presence of calorons/anticalorons we would here like to re-iterate [22, 39, 40] on technicalities in performing the effective loop expansion of the pressure in deconfining  $SU(2)$  Yang-Mills thermodynamics [21].

#### 3.1 Feynman rules and constraints

Following the extraction of the effective gauge coupling  $e(\lambda)$  from the thermodynamical consistency of effective, noninteracting quasiparticles, one may investigate the magnitude of radiative effects implied by the so-obtained function  $e(\lambda)$ . This strategy turns out to be selfconsistent. To perform the calculation we go back to supernatural units and work within the real-time formulation [14, 15, 16]. Thus  $\tilde{a}_\mu \rightarrow a_\mu$  etc.

The Feynman rules are formulated in the completely fixed (and physical) unitary-Coulomb gauge which avoids the consideration of Faddeev-Popov ghosts.

- For the three-vertex  $\Gamma_{[3]abc}^{\mu\nu\rho}(p, k, q)$  and for the four-vertex  $\Gamma_{[4]abcd}^{\mu\nu\rho\delta}(p, q, r, s)$ , we read

off from Eq. (12) that

$$\Gamma_{[3]abc}^{\mu\nu\rho}(p, k, q) = e(2\pi)^4 \delta(p + q + k) \varepsilon_{abc} [g^{\mu\nu}(q - p)^\rho + g^{\nu\rho}(k - q)^\mu + g^{\rho\mu}(p - k)^\nu], \quad (19)$$

$$\Gamma_{[4]abcd}^{\mu\nu\rho\delta}(p, q, r, s) = -ie^2(2\pi)^4 \delta(p + q + s + r) [\varepsilon_{fab} \varepsilon_{fcd} (g^{\mu\rho} g^{\nu\sigma} - g^{\mu\sigma} g^{\nu\rho}) + \varepsilon_{fac} \varepsilon_{fdb} (g^{\mu\sigma} g^{\rho\nu} - g^{\mu\nu} g^{\rho\sigma}) + \varepsilon_{fad} \varepsilon_{fbc} (g^{\mu\nu} g^{\sigma\rho} - g^{\mu\rho} g^{\sigma\nu})], \quad (20)$$

where  $\varepsilon_{abc}$  are the structure constants of SU(2).

- The propagator of the tree-level heavy (TLH) modes propagates thermalized on-shell particles (no energy-momentum transfer to  $\phi$  in the summation of the Dyson series for the interaction of  $a_\mu^{1,2}$  with  $\phi$ ) of mass  $m = 2e|\phi|$  only [16]

$$D_{\mu\nu,ab}^{\text{TLH}}(p) = -2\pi \delta_{ab} \tilde{D}_{\mu\nu} \delta(p^2 - m^2) n_B \left( \frac{|p^0|}{T} \right), \quad (21)$$

$$\tilde{D}_{\mu\nu} = \left( g_{\mu\nu} - \frac{p_\mu p_\nu}{m^2} \right). \quad (22)$$

The propagation of tree-level massless (TLM) modes splits into a vacuum and a thermal part:

$$D_{\mu\nu,ab}^{\text{TLM}}(p) = -\delta_{ab} \left\{ P_{\mu\nu}^T \left[ \frac{i}{p^2} + 2\pi \delta(p^2) n_B \left( \frac{|p^0|}{T} \right) \right] - \frac{i u_\mu u_\nu}{\mathbf{p}^2} \right\}, \quad (23)$$

where

$$P_T^{00} = P_T^{0i} = P_T^{i0} \equiv 0, \quad P_T^{ij} = \delta^{ij} - \frac{p^i p^j}{\mathbf{p}^2}. \quad (24)$$

Here  $n_B(x) = \frac{1}{e^x - 1}$  denotes the Bose-Einstein distribution function. Notice that TLM modes have a color index  $a = 3$  and TLH modes  $a = 1$  or  $a = 2$ . Moreover, the term  $\propto u_\mu u_\nu$  in Eq. (23) expresses the instantaneous “propagation” of the  $a_0^3$  field (Coulomb term<sup>11</sup>), and  $u_\mu = (1, 0, 0, 0)$  represents the four-velocity of the heat bath.

- The maximal off-shellness of a TLM mode with four-momentum  $p$  is constrained as [14, 21, 16]:

$$|p^2| \leq |\phi|^2 \quad (\text{TLH modes}) \quad |p^2| \leq |\phi|^2 \quad (\text{TLM modes}). \quad (25)$$

For a four-vertex with ingoing four-momenta  $p_1, p_2$  and outgoing four-momenta  $p_3, p_4$  we have [15, 21, 16]

$$\begin{aligned} |(p_1 + p_2)^2| &\leq |\phi|^2 \quad (\text{s-channel}), & |(p_3 - p_1)^2| &\leq |\phi|^2 \quad (\text{t-channel}), \\ |(p_3 - p_2)^2| &\leq |\phi|^2 \quad (\text{u-channel}). \end{aligned} \quad (26)$$

---

<sup>11</sup>However, one-loop radiatively induced, the emergence of longitudinally propagating  $E$ -field (charge-density) waves is observed [24].

As we shall review [21, 22] in Sec. 3.2, conditions (25), (26), and the requirement of on-shellness of TLH modes imply a rapid growth of the number of constraints over the number of a priori noncompact (radial) integration variables with an increasing number of loops in an irreducible diagram.

### 3.2 Expectations for convergence properties of loop expansion from two- and three-loop corrections to the pressure

As discussed in the previous section, the momentum transfer in all Mandelstam variables  $s, t$ , and  $u$  in a four-vertex with ingoing four-momenta  $p_1, p_2$  and outgoing four-momenta  $p_3, p_4$  should not exceed the scale  $|\phi|$ . For three-loop diagrams, and in particular the ones of Fig. 3, where the cutting of any line yields a 1Pi irreducible contribution to a polarization tensor, the number  $\tilde{K}$  of independent, radial loop-momentum variables  $(p_0, |\mathbf{p}|)_i$  for  $i = 1, 2, 3$  is  $\tilde{K} = 6$ . To judge the number  $K$  of independent constraints imposed on them we, in addition to (25) and (26), to consider on-shellness constraints for the TLH modes:

$$p_1^2 = m^2, \quad p_2^2 = m^2, \quad p_3^2 = m^2, \quad p_4^2 = (p_1 + p_2 - p_3)^2 = m^2. \quad (27)$$

Conditions (26) and (27) together yield for irreducible three-loop diagrams A and B a total of  $K = 3 + 4 = 7$  constraints.

According to (25), the TLM modes in the irreducible three-loop diagram C are subject to the maximal off-shellness conditions

$$|p_1^2| \leq |\phi|^2, \quad |p_2^2| \leq |\phi|^2, \quad (28)$$

and the on-shellness relations for the TLH modes in diagram C are

$$p_3^2 = m^2, \quad p_4^2 = (p_1 + p_2 - p_3)^2 = m^2. \quad (29)$$

Thus, again, we have  $K = 3 + 4 = 7$  constraints for diagram C. Hence for all irreducible three-loop diagrams we have  $K = 7$ . Therefore, the number of constraints exceeds the number of radial variables:

$$\tilde{K} < K. \quad (30)$$

This relation implies that irreducible three-loop integrations have either compact or empty supports.

For the two-loop diagrams of Fig. 2, we have  $\tilde{K} > K$ . Namely, the number of  $\tilde{K}$  of independent radial loop momenta  $(p_0, |\mathbf{p}|)_i$  for  $i = 1, 2$  is  $\tilde{K} = 4$  whereas the constraints plus the on-shellness conditions are

$$|(p_1 + p_2)^2| \leq |\phi|^2, \quad p_1^2 = m^2, \quad p_2^2 = m^2. \quad (31)$$

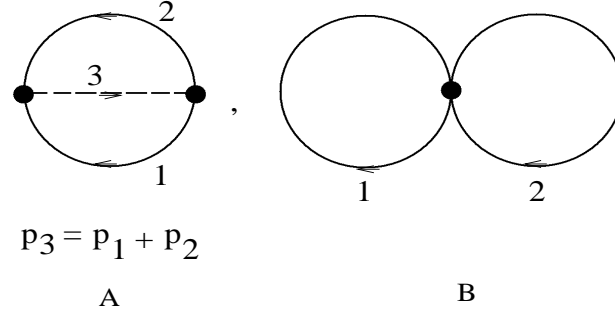


Figure 2: Two out of three nonvanishing two-loop diagrams with TLH (solid) and TLM (dashed) modes in the loops.

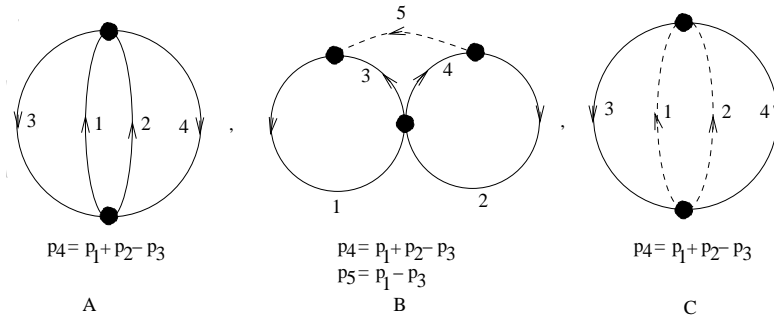


Figure 3: The three irreducible, planar three-loop diagrams with TLH (solid) and TLM (dashed) modes in the loops.

This implies  $K = 1 + 2 = 3$ . Thus, unlike the case of irreducible three-loop integrations, we expect the support of two-loop integrations to be noncompact. In Ref. [21] a counting of  $\tilde{K}$  versus  $K$  was performed for an arbitrary loop number in the case of planar and nonplanar irreducible loop diagrams which gives rise to the conjecture that, modulo resummations of irreducible contributions to the polarization tensors in the lines of a given bubble diagram, the expansion of the pressure *terminates* at a finite loop order. The fact that  $\tilde{K} < K$  [22] is already in agreement with this conjecture.

In the remaining subsections of Sec. 3 we discuss how numerical results are obtained and that, compared to the free quasiparticle pressure, two-loop and irreducible three-loop diagrams exhibit a hierarchical suppression of their contributions to the thermodynamical pressure [22]. In fact, diagram C of Fig. 3 is shown to vanish.

### 3.3 Irreducible 3-loop integrations

For the irreducible three-loop bubble diagrams in Fig. 3, we have in case A two four-vertices and four propagators and the correction to the pressure is

$$\Delta P_A = \frac{1}{48} \int \frac{d^4 p_1 d^4 p_2 d^4 p_3}{(2\pi)^4 (2\pi)^4 (2\pi)^4} \Gamma_{[4]abcd}^{\mu\nu\rho\sigma} \Gamma_{[4]\bar{a}\bar{b}\bar{c}\bar{d}}^{\bar{\mu}\bar{\nu}\bar{\rho}\bar{\sigma}} D_{\rho\bar{\rho},c\bar{c}}(p_1) D_{\sigma\bar{\sigma},d\bar{d}}(p_2) \quad (32)$$

$$\times D_{\mu\bar{\mu},a\bar{a}}(p_3) D_{\nu\bar{\nu},b\bar{b}}(p_4),$$

where the momenta are subject to the constraints (26) and (27) and overall momentum conservation has been used ( $p_4$  is a function of  $p_1, p_2, p_3$ ).

For diagram B we have one four-vertex, two three-vertices and five propagators. Therefore, the correction to the pressure is

$$\Delta P_B = \frac{1}{2} \int \frac{d^4 p_1 d^4 p_2 d^4 p_3}{(2\pi)^4 (2\pi)^4 (2\pi)^4} \Gamma_{[4]hijk}^{\alpha\beta\gamma\lambda} \Gamma_{[3]abc}^{\mu\nu\rho} \Gamma_{[3]\bar{a}\bar{b}\bar{c}}^{\bar{\mu}\bar{\nu}\bar{\rho}} D_{\mu\alpha,ah}(p_1) D_{\bar{\mu}\bar{\beta},\bar{a}\bar{i}}(p_2) \quad (33)$$

$$\times D_{\gamma\rho,jc}(p_3) D_{\lambda\bar{\rho},k\bar{c}}(p_4) D_{\mu\bar{\nu},b\bar{b}}(p_5),$$

where the momenta are subject to same constraints as in diagram A. It should be noticed that for the massless mode,  $p_5 = p_1 - p_3$ , we do not need to consider an additional constraint  $|p_5|^2 \leq |\phi|^2$  because this constraint is automatically satisfied by the t-channel condition in (26).

For diagram C, the Feynman rules are similar to diagram A and the correction to the pressure is

$$\Delta P_C = \frac{1}{48} \int \frac{d^4 p_1 d^4 p_2 d^4 p_3}{(2\pi)^4 (2\pi)^4 (2\pi)^4} \Gamma_{[4]abcd}^{\mu\nu\rho\sigma} \Gamma_{[4]\bar{a}\bar{b}\bar{c}\bar{d}}^{\bar{\mu}\bar{\nu}\bar{\rho}\bar{\sigma}} D_{\rho\bar{\rho},c\bar{c}}(p_1) D_{\sigma\bar{\sigma},d\bar{d}}(p_2)$$

$$\times D_{\mu\bar{\mu},a\bar{a}}(p_3) D_{\nu\bar{\nu},b\bar{b}}(p_4), \quad (34)$$

where the momenta are subject to the constraints (26), (28), and (29).

Now, insert the Feynman rules (19) - (23) in the above integrals (32) - (34), consider the dimensionless variables  $x_i \equiv \frac{|\mathbf{p}_i|}{|\phi|}$  ( $i = 1, 2, 3$ ) for rescaling the radial loop momenta, and consider the following steps:

- Carry out Lorenz and color contractions.
- Go over to 3D spherical coordinates.
- Trivially integrate the temporal components of four-momenta by appealing to the delta functions of the propagators.
- Apply the triangle inequality to obtain upper bounds for the modulus of each correction.

For the corrections (32) and (33) we obtain the following expressions

$$\begin{aligned}
|\Delta P_{A(B)}| \leq & (24) \frac{e^4 \Lambda^4 \lambda^{-2}}{3 \times 2^7 \times (2\pi)^6} \sum_{l,m,n=1}^2 \int dx_1 \int dx_2 \int dx_3 \int dz_{12} \int dz_{13} \int_{z_{23,l}}^{z_{23,u}} dz_{23} \\
& \times \frac{1}{\sqrt{(1-z_{12}^2)(1-z_{13}^2) - (z_{23} - z_{12}z_{13})^2}} \\
& \times \frac{x_1^2 x_2^2 x_3^2}{\sqrt{x_1^2 + 4e^2} \sqrt{x_2^2 + 4e^2} \sqrt{x_3^2 + 4e^2}} \\
& \times \delta(4e^2 + ((-1)^{l+m} \sqrt{x_1^2 + 4e^2} \sqrt{x_2^2 + 4e^2} - x_1 x_2 z_{12} - \\
& ((-1)^{l+n} \sqrt{x_1^2 + 4e^2} \sqrt{x_3^2 + 4e^2} - x_1 x_3 z_{13}) - \\
& ((-1)^{m+n} \sqrt{x_2^2 + 4e^2} \sqrt{x_3^2 + 4e^2} - x_2 x_3 z_{23})) \\
& \times |P_{A(B)}(x, z, l, m, n)| n_B(2\pi \lambda^{-3/2} \sqrt{x_1^2 + 4e^2} \times \\
& n_B(2\pi \lambda^{-3/2} \sqrt{x_2^2 + 4e^2} n_B(2\pi \lambda^{-3/2} \sqrt{x_3^2 + 4e^2} \times \\
& n_B(2\pi \lambda^{-3/2} |(-1)^l \sqrt{x_1^2 + 4e^2} + (-1)^m \sqrt{x_2^2 + 4e^2} + \\
& (-1)^n \sqrt{x_3^2 + 4e^2}|, \tag{35}
\end{aligned}$$

where  $z_{12} \equiv \cos \angle(\mathbf{x}_1, \mathbf{x}_2)$ ,  $z_{13} \equiv \cos \angle(\mathbf{x}_1, \mathbf{x}_3)$ ,  $z_{23} \equiv \cos \angle(\mathbf{x}_2, \mathbf{x}_3)$ . The extremely lengthy polynomials  $P_A$  and  $P_B$  arise from Lorenz and color contractions and are regular at  $x_1 = x_2 = x_3 = 0$ . We also define [21]:

$$z_{23,u} \equiv \cos |\arccos z_{12} - \arccos z_{13}|, \quad z_{23,l} \equiv \cos |\arccos z_{12} + \arccos z_{13}|. \tag{36}$$

Recalling (27) and the fact that only the minus sign is relevant ( $e > \frac{1}{2\sqrt{2}}$ ) [40], which makes the expression within the absolute-value signs strictly negative, we



have

$$z_{12} \leq \frac{1}{x_1 x_2} (4e^2 - \sqrt{x_1^2 + 4e^2} \sqrt{x_2^2 + 4e^2} + \frac{1}{2}) \equiv g(x_1, x_2) \quad (37)$$

$$z_{13} \geq \frac{1}{x_1 x_3} (-4e^2 + \sqrt{x_1^2 + 4e^2} \sqrt{x_3^2 + 4e^2} - \frac{1}{2}) \equiv g(x_1, x_3) \quad (38)$$

$$z_{23} \geq \frac{1}{x_2 x_3} (-4e^2 + \sqrt{x_2^2 + 4e^2} \sqrt{x_3^2 + 4e^2} - \frac{1}{2}) \equiv g(x_2, x_3). \quad (39)$$

Repeating the same steps as before, for the vacuum-vacuum contribution (34) of diagram C we obtain

$$\begin{aligned} |\Delta P_C| \leq & \frac{e^4 \Lambda^4 \lambda^{-2}}{3 \times 2^5 \times (2\pi)^8} \sum_{l,m}^2 \int dy_1 \int dx_1 \int dx_2 \int dx_3 \int dz_{12} \int dz_{13} \int_{z_{23,l}}^{z_{23,u}} dz_{23} \\ & \times \frac{x_1^2 x_2^2 x_3^2}{\sqrt{(1 - z_{12}^2)(1 - z_{13}^2) - (z_{23} - z_{12} z_{13})^2}} \\ & \times |P_C(\mathbf{x}, \mathbf{z}, y_1, l, m)| n_B (2\pi \lambda^{-3/2} \sqrt{x_3^2 + 4e^2}) \\ & \times \frac{n_B (2\pi \lambda^{-3/2} |(-1)^l \sqrt{x_3^2 + 4e^2} + (-1)^m f_2(\mathbf{x}, \mathbf{z})|)}{f_2(\mathbf{x}, \mathbf{z}, y_1) \sqrt{x_3^2 + 4e^2}}, \end{aligned} \quad (40)$$

where

$$f_2(\mathbf{x}, \mathbf{z}) \equiv \sqrt{x_1^2 + x_2^2 + x_3^2 + 2x_1 x_2 z_{12} - 2x_1 x_3 z_{13} - 2x_2 x_3 z_{23}}, \quad y_1 \equiv \frac{p_1^o}{|\phi|}, \quad (41)$$

with  $z_{12}, z_{13}, z_{23}, z_{23,u}$ , and  $z_{23,l}$  defined in (37),(38),(39) and (36), respectively. The polynomial  $P_C$  emerges from Lorenz and color contractions and is regular at  $x_1 = x_2 = x_3 = 0$ . According to relation (26) - (28) the rescaled constraints read:

$$|y_1^2 + y_2^2 - x_1^2 - x_2^2 + y_1 y_2 - 2x_1 x_2 z_{12}| \leq 1, \quad (42)$$

$$|y_2^2 - x_2^2 + 4e^2 - (-1)^l 2y_2 \sqrt{x_3^2 + 4e^2} + 2x_2 x_3 z_{23}| \leq 1, \quad (43)$$

$$|y_1^2 - x_1^2 + 4e^2 - (-1)^l 2y_1 \sqrt{x_3^2 + 4e^2} + 2x_1 x_3 z_{13}| \leq 1, \quad (44)$$

$$|y_1^2 - x_1^2| \leq 1, \quad |y_2^2 - x_2^2| \leq 1. \quad (45)$$

Moreover,  $y_2$  is replaced by

$$y_2 = -y_1 + 2(-1)^l \sqrt{x_3^2 + 4e^2} + (-1)^m f_2(\mathbf{x}, \mathbf{z}), \quad (46)$$

through delta function integration, and  $(l, m = 1, 3)$ .

### 3.4 Monte-Carlo integration of irreducible 3-loop diagrams

#### 3.4.1 Monte-Carlo integration in general

In the following we briefly discuss how the integral of a function  $f$  over a region  $G \subset \mathbb{R}^n$  can be calculated using statistical methods. Du to the complexity of the region (algebraic varieties)  $G$  that support<sup>12</sup> a three-loop integration, statistical methods are required in a numerical computations of the values of bubble diagrams A, B, and C in Fig.3. Its characteristic function is denoted by  $\chi_G$ . The integral then reads

$$\int_G f(x)dx = \int_{\mathbb{R}^n} \chi_G(x)f(x)dx. \quad (47)$$

If  $G$  is compact then it can be included in a box  $B = [x_1, X_1] \times [x_2, X_2] \times \dots \times [x_n, X_n]$ . Therefore the integral in Eq. (47) can be written as

$$\int_{\mathbb{R}^n} \chi_G(x)f(x)dx = \int_B \chi_G(x)f(x)dx. \quad (48)$$

If  $B$  has volume  $V$ ,  $\frac{1}{V}\chi_B$  can be considered as the probability density function of a random variable  $X$ , which is equally distributed throughout the box  $B$ . The integral then is exactly the expectation value  $E(V\chi_G(X)f(X))$

$$\int_B \chi_G(x)f(x)dx = V \int_B \chi_G(x)f(x)\frac{1}{V}\chi_B dx = VE(\chi_G(X)f(X)). \quad (49)$$

The Monte-Carlo method to calculate this integral consists of a statistical estimate of the expectation value. It is well known that the mean value  $\bar{X}$  of a sample is an unbiased estimator for the expected value. If one draws a random sample  $(x_1, x_2, \dots, x_n)$  of points from the box, the estimate becomes:

$$\int_G f(x)dx \approx V \frac{1}{n} \sum_{i=1}^n \chi_G(x_i)f(x_i). \quad (50)$$

The Monte-Carlo-Method is particularly useful to determine integrals over high-dimensional integration regions, where deterministic methods would be too time consuming. Unfortunately, the precision of this statistical estimate increases only with the root of the sample size. For example, this implies that the Monte-Carlo method is a relatively fast way to achieve a result with a relative precision of about 1 percent, but to achieve one more decimal place in the result the sample size must be increased by a factor of 100.

#### 3.4.2 Monte-Carlo integration for diagrams A and B

The calculation of  $\Delta P_A$  and  $\Delta P_B$  includes an integration over a six-dimensional region  $G$  with variables of integration<sup>13</sup>  $x_1, x_2, x_3, z_{12}, z_{13}, z_{23}$ . As  $z_{ij} \equiv \cos \angle(\mathbf{x}_i, \mathbf{x}_j)$ ,

<sup>12</sup>The region  $G$  is determined by a set of inequalities.

<sup>13</sup>Notice that  $x_1$  is integrated analytically through the delta function in  $\Delta P_A$  and  $\Delta P_B$ .

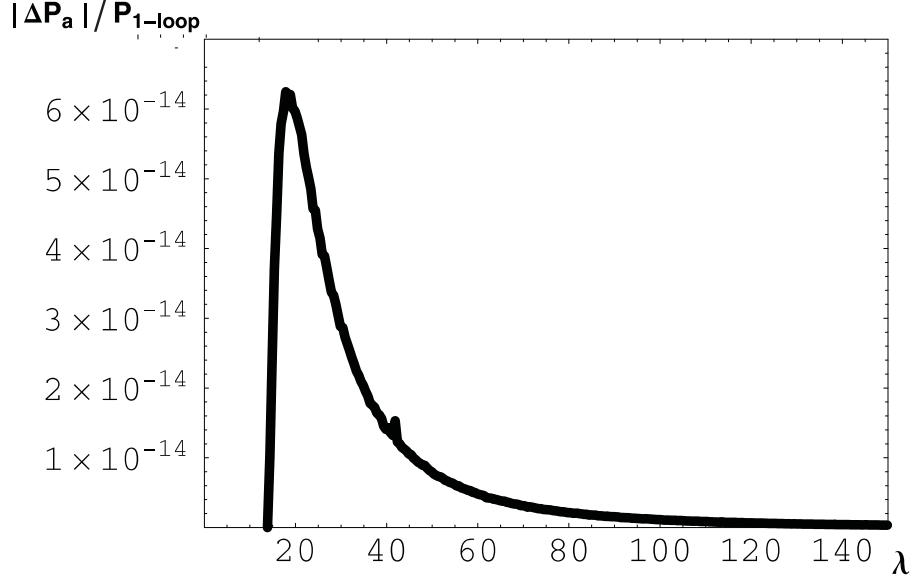


Figure 4: Upper estimate for the modulus  $\frac{1}{24}|\Delta P_A|/P_{1\text{-loop}}$  as a function of  $\lambda$  for diagram A in Fig. 3.

their range is restricted to the interval  $[-1, 1]$ . The exact shape of  $G$  is then determined by the constraints (37) - (39) and an additional angular condition (36) on  $z_{23}$ . This angular condition allows for a further reduction of the range of  $z_{23}$  to the interval  $[z_{23,l}, z_{23,u}]$ . Also, the constraints (37) - (39) and condition (37) restrict the  $x_i$  to the interval  $[0, 3]$  [21]. Therefore a box  $B$  which contains  $G$  is identified. The constraints define the characteristic function  $\chi_G$  whereas  $z_{23,l}$  and  $z_{23,u}$  are used directly as integration limits. According to this, the ratios of the moduli  $\Delta P_A$  and  $\Delta P_B$  to the one-loop (ground-state subtracted) approximation are computed as a function of the dimensionless temperature  $\lambda_c = 13.87 \leq \lambda \equiv \frac{2\pi T}{\Lambda} \leq 140$ , and the results are represented in Fig. 4–7. For the effective gauge coupling the solution of the one-loop evolution equation (7) is used. Figs. 4 - 7 show that at the critical temperature  $\lambda_c = 13.87$  there is no loop correction (decoupling of TLH modes), and  $\Delta P_A$  and  $\Delta P_B$  approach zero for large temperatures. For the three-loop diagrams A and B, the maxima of the ratio of the estimates of their moduli to the one-loop correction are peaked between  $\lambda = 17.5$  and  $\lambda = 20$ . They are  $6 \cdot 10^{-14}$  and  $2 \cdot 10^{-7}$ , respectively. This shows the dominance of diagram B. (The next section suggests that diagram C is vanishing). Comparing Fig. 5 with Fig. 6 and Fig. 7, shows the dominance of Coulomb fluctuations ( $10^{-7}$ ) over quantum fluctuation ( $10^{-12}$ ) for in the TLM propagation contributing to diagram B.

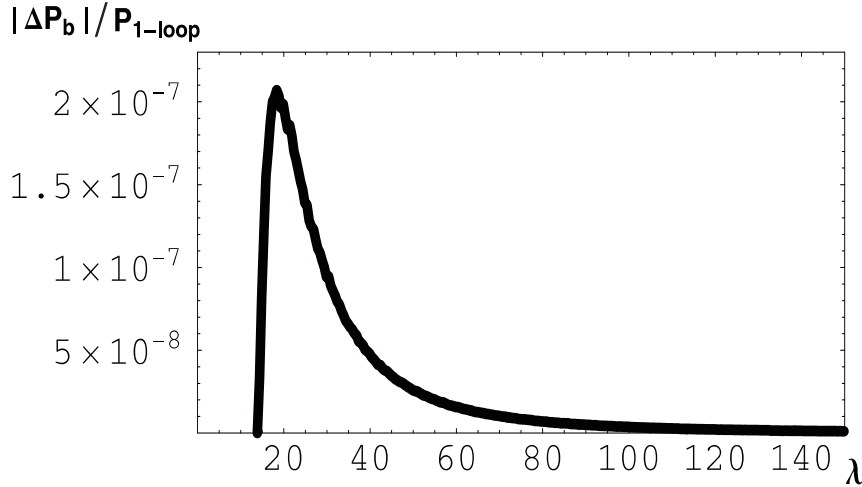


Figure 5: Total upper estimate for the modulus  $\frac{1}{24}|\Delta P_B|/P_{1\text{-loop}}$  as a function of  $\lambda$  for diagram B in Fig. 3.

### 3.4.3 Monte-Carlo integration of diagram C

The region of support for the radial loop integration the irreducible three-loop diagram C cannot be determined in the same way as for diagrams A and B. This has mainly to do with the occurrence of additional off-shell variables. In order to estimate the region of loop integration  $G$  for diagram C, we consider a box with volume  $10 \times 10 \times 10 \times 20 \times 2 \times 2 \times 2$  for the loop and angular variables  $x_1, x_2, x_3, y_1, z_{12}, z_{13}, z_{23}$ , respectively. Through the condition  $|y_1^2 - x_1^2| \leq 1$ , and the definition of  $z_{23,(u,l)}$  in Eq. (36) a subregion of this volume is determined, which roughly represents 2 % of the volume of the box. In this subset 150,000,000 points are randomly picked. Subsequently, it is checked whether the conditions (42) - (46). With 600,000,000 tests we have not found a single point to satisfy all these conditions. This yields an estimate of a fraction of about  $2 \times 10^{-5}$  of the box volume for the region of integration. The typical distance between the sampled point is  $0.2 \sim \sqrt[3]{2 \times 10^{-5}}$ . Thus it is highly probable that the region of integration is empty. A similar analysis applies to the vacuum-thermal combination of TLM propagators, and the constraints imply that the integration region is empty provided the region of integration for the vacuum-vacuum combination is empty. Again, we have gathered compelling evidence for the latter to be true.

## 3.5 Comparison to 2-loops results, hierarchy

In order to check the reliability of our numerical method in case of three-loop integrations, we compute the pressure of the two-loop diagram B in Fig. 2 with the Monte-Carlo method and compare the result with results obtained by deterministic means [39, 40].

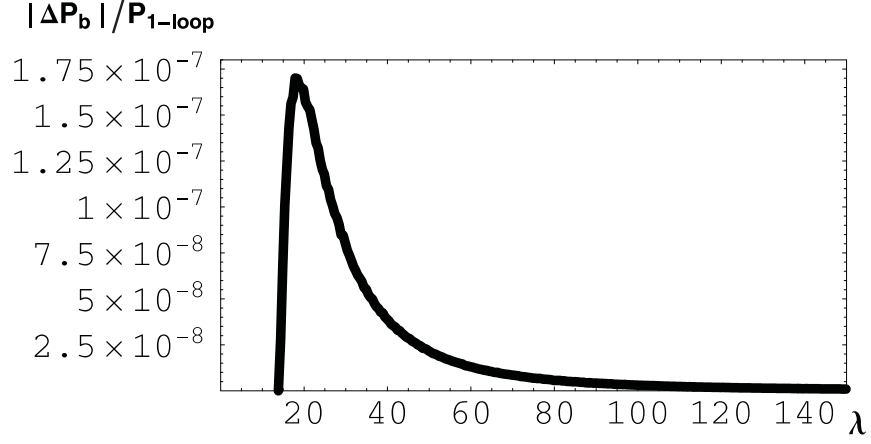


Figure 6: Upper estimate for the modulus of  $\frac{1}{24}|\Delta P_B|/P_{1\text{-loop}}$  due to the Coulomb part of the TLM propagator as a function of  $\lambda$  for diagram B.

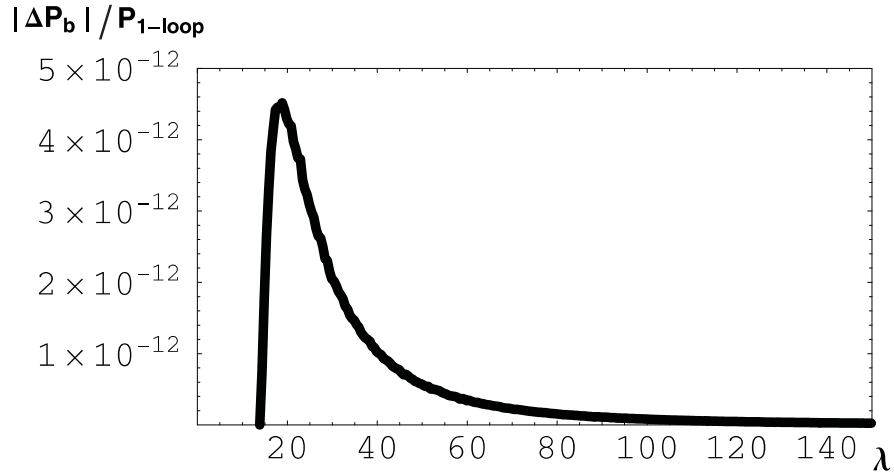


Figure 7: Upper estimate for the modulus of  $\frac{1}{24}|\Delta P_B|/P_{1\text{-loop}}$  due to TLM quantum fluctuations as a function of  $\lambda$  for diagram B.

For the two-loop diagram B in Fig. 2, we have two-propagators and one four-vertex at which the momenta are subject to the s-channel constraint constraint in (26). Thus the two-loop correction to the free quasiparticle pressure arising from diagram B takes the form

$$\Delta P_B = \frac{1}{i} \int \frac{d^4 p d^4 k}{(2\pi)^8} \Gamma_{[4]abcd}^{\mu\nu\rho\delta} D_{\mu\nu,ab}(p) D_{\rho\delta,cd}(k), \quad (51)$$

where

$$|(p+k)^2| \leq |\phi|^2. \quad (52)$$

As before, we can rescale the momenta as  $x \equiv \frac{|\mathbf{p}|}{|\phi|}$  and  $y \equiv \frac{|\mathbf{k}|}{|\phi|}$  and obtain

$$\begin{aligned} \Delta P_B = & -\frac{e^2 \Lambda^4 \lambda^{-2}}{2(2\pi)^4} \int dx \int dy \int dz_{xy} \frac{x^2 y^2}{\sqrt{x^2 + 4e^2} \sqrt{y^2 + 4e^2}} \\ & \times P_B(x, y, z_{xy}) n_B(2\pi\lambda^{-3/2} \sqrt{x^2 + 4e^2}) n_B(2\pi\lambda^{-3/2} \sqrt{y^2 + 4e^2}), \end{aligned} \quad (53)$$

where

$$z_{xy} \leq \frac{1}{xy} (4e^2 - \sqrt{x^2 + 4e^2} \sqrt{y^2 + 4e^2} + \frac{1}{2}) \equiv g(x, y). \quad (54)$$

Notice that

$$\lim_{x,y \rightarrow \infty} g(x, y) = -1. \quad (55)$$

In (52) only the minus sign is relevant since  $e > \frac{1}{2\sqrt{2}}$ , and therefore the expression within the absolute-value signs is strictly negative. This leads to (54). Apart from a small compact region, where  $g(x, y) \geq 1$  and which includes the origin  $x = y = 0$  in the  $(x \geq 0, y \geq 0)$ -quadrant, the admissible region of  $x, y$ -integration ( $-1 \leq g(x, y) \leq +1$ ) is an infinite strip bounded by two functions:

$$y^u(x) \equiv \frac{x + 8e^2 + \sqrt{1 + 16e^2} \sqrt{x^2 + 4e^2}}{8e^2}, \quad (56)$$

$$y^l(x) \equiv \frac{x + 8e^2 - \sqrt{1 + 16e^2} \sqrt{x^2 + 4e^2}}{8e^2}. \quad (57)$$

We now use the Monte-Carlo Method to calculate diagram B. In order to bound the region we restrict the arguments of the Bose-factors to the following interval:

$$0 \leq 2\pi\lambda^{-3/2} \sqrt{x^2 + 4e^2} \leq 10 \quad (58)$$

and

$$0 \leq 2\pi\lambda^{-3/2} \sqrt{y^2 + 4e^2} \leq 10. \quad (59)$$

These restrictions ensure that no Boltzmann tails are included in the region of radial loop integration. The integrand of (53) is plotted in Fig. 8 below. It is clear from Fig. 8 that the support for the  $x$  and  $y$  integrations is an infinite strip in the  $x$ - $y$

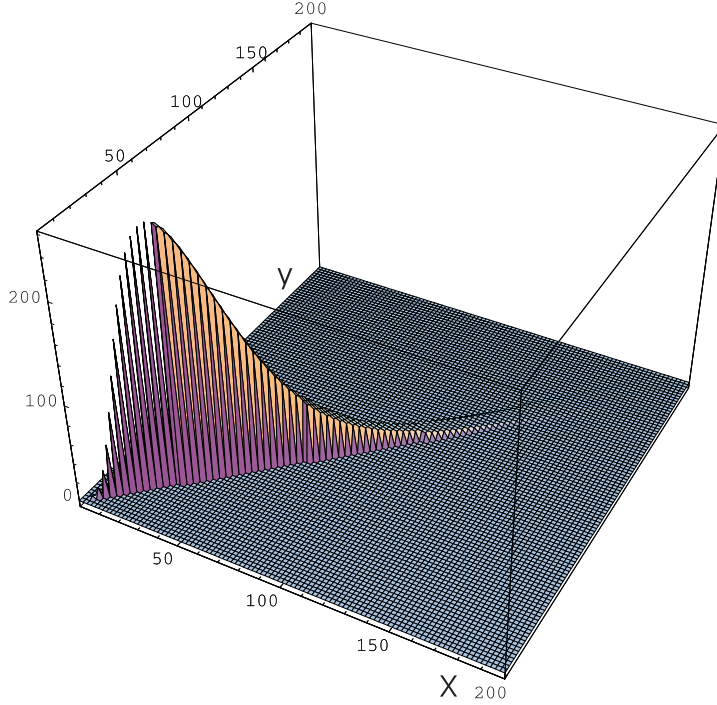


Figure 8: The integrand in Eq.(53) plotted as a function of  $x$  and  $y$  for fixed  $z_{xy} \equiv \cos \angle(\mathbf{x}, \mathbf{y})$ . The horizontal plane represents the  $x$ - $y$  plane where the integrand (mountain-shaped object) stands on an infinite strip.

plane. From  $x = y = 150$  on suppressions are severe justifying the limits taken in (58) and (59). For instance, by taking  $x = y = 150, e = \sqrt{8}\pi$  and  $\lambda = 30$ , we obtain  $2\pi\lambda^{-3/2}\sqrt{x^2 + 4e^2} \sim 5.77$ . The ratio of two-loop to one-loop, as computed by the Monte-Carlo method, is represented in Fig.9. There are no significant deviations from the deterministic results computed in [39, 40]. Both estimates are of order  $10^{-6}$  at temperatures  $\lambda = 20 \pm 5$ . Let us now compare the integrand of (53), illustrated in Fig.8 for the two-loop diagram B, with the integrand of (35), illustrated in Fig.10 for the three-loop diagram B.

To obtain an idea about the shape of the region of radial loop integration for the three-loop diagram B we adopt the following procedure. We use a grid of cosine values for  $z_{12}$ ,  $z_{13}$ , and  $z_{23}$  of 0.15 separation. This amounts to approximatively 2300 points. For each point we compute the modulus of the integrand as a function of  $x_2$  and  $x_3$ ; the  $x_1$ -integration can be performed trivially by appealing to the  $\delta$ -function in the integrand. Subsequently, a sum over all grid points is performed, and Fig.10 depicts the result of this summation and the  $x_1$  integration. The  $x_2$ - $x_3$  region of integration is the area where this result does not vanish. Fig.10 supports the claim in [21] that the region of radial loop integration in the three-loop case is compact. The fact that the upper limits of integration for  $x_2$  and  $x_3$  have been set to 3 shows that this region is fully covered in the Monte-Carlo process.

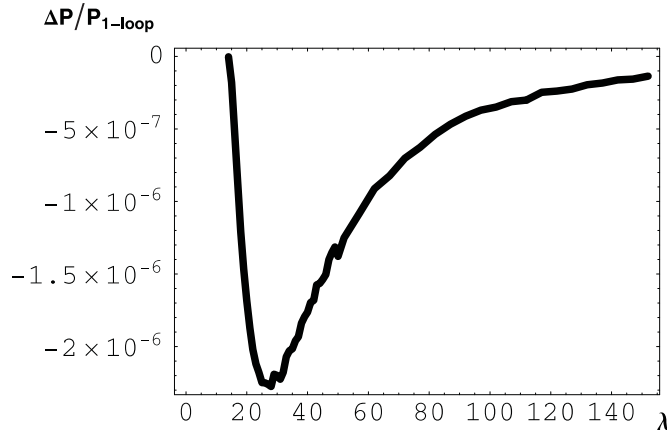


Figure 9: The ratio of  $\Delta P_B$  (2-loop) and  $P_{1-loop}$  plotted for  $13.87 \leq \lambda \leq 140$ .

Recall that Fig. 8 shows the integrand for the two-loop diagram for a particular choice of the cosine value  $z_{xy}$  close to  $-1$ . The region of radial loop integration is obviously not compact. However, the integrand is Boltzmann suppressed for large  $x$  and  $y$ .

The remarkable contrast between the two-loop and irreducible, planar three-loop diagrams can be seen from Fig. 8 and Fig. 10: in agreement with our counting of constraints in Sec. 3.2, the region of radial loop integration is compact in the latter while it is non-compact in the former case. The numerical results [40, 22], reviewed in Fig. 4 - 7 and Fig. 9, show that one-loop, two-loop, and irreducible three-loop corrections are hierarchically ordered with a pronounced suppression at increasing loop order. In particular, comparing the modulus of the dominant irreducible three-loop correction with the smallest two-loop correction, we infer that they are comparable at their maxima in  $\lambda$ . On the other hand, comparing it with the dominant two-loop correction, shows a minimal suppression by a factor of  $\sim 10^{-3}$ . The dominant irreducible three-loop contribution is significantly dominated by Coulomb fluctuations, and the other nonvanishing irreducible three-loop contribution is minimally suppressed by a factor  $10^{-11}$  compared to the dominant two-loop contribution. Also, recall that one three-loop diagram appears to vanish exactly. These results provide numerical evidence for the conjecture [21] on the termination of expansion of thermodynamical quantities or polarization tensors into irreducible loops (modulo resummation of reducible diagrams) to be true <sup>14</sup>.

---

<sup>14</sup>As discussed in [21], constraints on the loop-integration variables in nonplanar, irreducible bubble diagrams are more severe than in the here-discussed planar case.



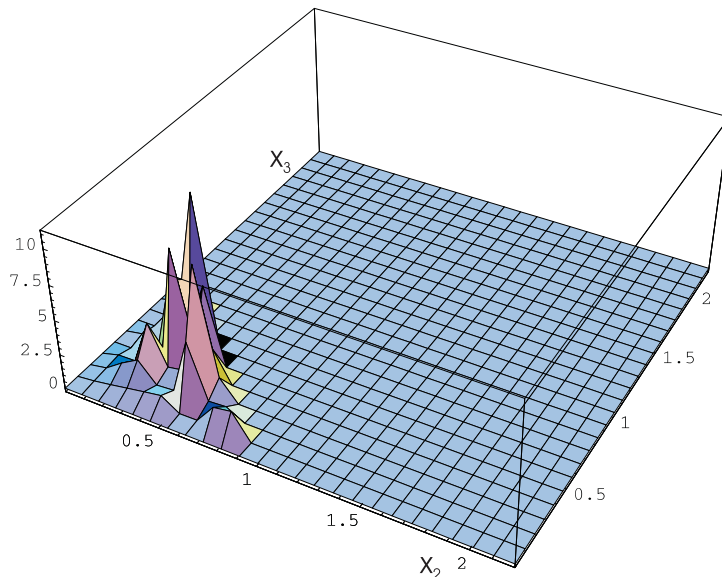


Figure 10: The result of  $x_1$ -integration and summation over a grid of cosine values  $z_{12} \equiv \cos \angle(\mathbf{x}_1, \mathbf{x}_2)$ ,  $z_{13} \equiv \cos \angle(\mathbf{x}_1, \mathbf{x}_3)$ , and  $z_{23} \equiv \cos \angle(\mathbf{x}_2, \mathbf{x}_3)$  of the integrand in Eq. (35) plotted as a function of  $x_2$  and  $x_3$ , see text.

## 4 Summary

In this work we have addressed the question how the universality of the quantum of action  $\hbar$  may find an explanation in terms of the Euclidean action of nonpropagating, selfdual gauge-field configurations of an  $SU(2)$  Yang-Mills theory and, after interpreting these configurations as the inducers of local vertices between plane waves, how the radiative correction of the full theory become finite. Recall that in perturbation theory, where the topologically nontrivial sector of field configurations is ignored, ultraviolet divergences are removed by a conditioned subtraction. We have pointed out that this pragmatism of renormalization theory, which was proved a long time ago to be physically consistent [9, 10], is justified by solely a small window in scale parameter, associated with the just-not-resolved, relevant topological sector of the theory (calorons/anticalorons of topological charge modulus unity), inducing local vertices between plane waves. We also have discussed how the coupling of photons to electric charges is related to the dual of the effective gauge coupling in the deconfining phase. Finally, to illustrate the workings of effective loops we have made explicit certain technicalities of the effective pressure expansion in deconfining  $SU(2)$  Yang-Mills thermodynamics. Numerically, the hierarchical suppression of increasing loop orders supports the conjecture of a termination at a finite order of the expansion into irreducible diagrams [21].

## References

- [1] M. Planck, Ann. d. Phys. **309**, 553 (1901).
- [2] M. Planck, *Nobel Lecture* (1918).
- [3] L. de Broglie, *Recherches sur la thorie des quanta*, doctoral thesis (1924).
- [4] A. Einstein, Ann. d. Phys. **322**, 132 (1905).
- [5] N. Bohr, Philosoph. Magazine **26**, 1 (1913).  
N. Bohr, Philosoph. Magazine **26**, 476 (1913).  
N. Bohr, Philosoph. Magazine **26**, 857 (1913).  
N. Bohr, Nature **92**, 231 (1914).
- [6] W. Heisenberg, Z. Phys. **33**, 879 (1925).  
W. Heisenberg, Z. Phys. **43**, 172 (1927).
- [7] E. Schrödinger, Ann. d. Phys. **79**, 361 (1926).  
E. Schrödinger, Ann. d. Phys. **79**, 489 (1926).  
E. Schrödinger, Ann. d. Phys. **80**, 437 (1926).  
E. Schrödinger, Ann. d. Phys. **81**, 109 (1926).
- [8] *BCS: 50 years*, eds. L. N. Cooper and D. Feldman, World Scientific Publishing Company (2010).
- [9] G. 't Hooft and M. J. G. Veltman, Nucl. Phys. B **44**, 189 (1972).  
G. 't Hooft, Nucl. Phys. B **33**, 173 (1971).  
G. 't Hooft, Nucl. Phys. B **62**, 444 (1973).  
G. 't Hooft and M. J. G. Veltman, Nucl. Phys. B **50**, 318 (1972).
- [10] B. W. Lee and Jean Zinn-Justin, Phys. Rev. D **5**, 3121 (1972).  
B. W. Lee and Jean Zinn-Justin, Phys. Rev. D **5**, 3137 (1972).  
B. W. Lee and Jean Zinn-Justin, Phys. Rev. D **5**, 3155 (1972).
- [11] B. J. Harrington and H. K. Shepard, Phys. Rev. D **17**, 2122 (1978).
- [12] W. Nahm, Phys. Lett. B **90**, 413 (1980).  
W. Nahm, Lect. Notes in Physics. 201, eds. G. Denaro, e.a. (1984) p. 189.  
K.-M. Lee and C.-H. Lu, Phys. Rev. D **58**, 025011 (1998).  
T. C. Kraan and P. van Baal, Phys. Lett. B **428**, 268 (1998).  
T. C. Kraan and P. van Baal, Phys. Lett. B **435**, 389 (1998).
- [13] U. Herbst and R. Hofmann, accept. ISRN (2011). [hep-th/0411214]

- [14] R. Hofmann, Int. J. Mod. Phys. A **20**, 4123 (2005), Erratum-ibid. A **21**, 6515 (2006).  
R. Hofmann, Mod. Phys. Lett. A **21**, 999 (2006), Erratum-ibid. A **21**, 3049 (2006).
- [15] R. Hofmann, arXiv:0710.0962 [hep-th].
- [16] R. Hofmann, *The Thermodynamics of Quantum Yang-Mills theory*, World Scientific Publishing Company (2011).
- [17] R. Hofmann, *Symposium on ‘Analysis of Quantum Field Theories’*, 9th International Conference on Numerical Analysis and Applied Mathematics, AIP Conf. Proc. **1389**, 671 (2011).
- [18] J. Keller et al., Ann. d. Phys. **19**, 102 (2010).
- [19] M. Schwarz, *Symposium on ‘Analysis of Quantum Field Theories’*, 9th International Conference on Numerical Analysis and Applied Mathematics, AIP Conf. Proc. **1389**, 655 (2011).
- [20] D. Kaviani, *Symposium on ‘Analysis of Quantum Field Theories’*, 9th International Conference on Numerical Analysis and Applied Mathematics, AIP Conf. Proc. **1389**, 646 (2011).
- [21] R. Hofmann, accepted Braz. J. Phys. (2011). [hep-th/0609033]
- [22] D. Kaviani and R. Hofmann, Mod. Phys. Lett. A **22**, 2343 (2007).
- [23] C. Falquez, R. Hofmann, and T. Baumbach, arXiv:1009.1715 [hep-th].
- [24] C. Falquez, R. Hofmann, and T. Baumbach, arXiv:1106.1353 [hep-th].
- [25] J. Ludescher and R. Hofmann, Ann. Phys. **18**, 271 (2009).
- [26] F. Giacosa and R. Hofmann, Phys. Rev. D **76**, 085022 (2007).
- [27] D. J. Gross, R. D. Pisarski, and L. G. Yaffe, Rev. Mod. Phys. **53**, 43 (1981).
- [28] B. J. Harrington and H. K. Shepard, Phys. Rev. D **18**, 2990 (1978).
- [29] S. J. Brodsky and P. Hoyer, Phys. Rev. D **83**, 045026 (2011).
- [30] J. Iliopoulos, C. Itzykson, and A. Martin, Rev. Mod. Phys. **47**, 165 (1975).  
J. F. Donoghue et al., Phys. Lett. B **529**, 132 (2002).  
N. E. J. Bjerrum-Bohr, J. F. Donoghue, and B. R. Holstein, Phys. Rev. D **68**, 084005 (2003). [Erratum-ibid. D **71**, 069904 (2005)]  
B. R. Holstein and J. F. Donoghue, Phys. Rev. Lett. **93**, 201602 (2004).
- [31] F. Giacosa and R. Hofmann, Eur. Phys. J. C **50**, 635 (2007). [hep-th/0512184].

- [32] J. Moosmann and R. Hofmann, arXiv:0807.3266 [hep-th].
- [33] D. Diakonov et al., Phys. Rev. D **70**, 036003, (2004).
- [34] G. 't Hooft, Phys. Rev. Lett. **37**, 8 (1976).
- [35] G. 't Hooft, Phys. Rev. D **14**, 3432 (1976).
- [36] R. Hofmann, Ann. Phys. **18**, 634 (2009).
- [37] J. Moosmann and R. Hofmann, arXiv:0804.3527 [hep-th].
- [38] R. Hofmann, Mod. Phys. Lett. A **22**, 2657 (2007).
- [39] U. Herbst, R. Hofmann, and J. Rohrer, Acta Phys. Polon. B **36**, 881 (2005).
- [40] M. Schwarz, R. Hofmann, and F. Giacosa, Int. J. Mod. Phys. A **22**, 1213 (2007).